Catalysis Today 154 (2010) 217–223

Contents lists available at ScienceDirect

Catalysis Today

journal homepage: www.elsevier.com/locate/cattod

Kinetics of carbon nanotubes growth on a Ni–Mg–Al catalyst by CCVD of methane: Influence of catalyst deactivation

N. Latorre, E. Romeo, J.I. Villacampa, F. Cazaña, C. Royo, A. Monzón*

Institute of Nanoscience of Aragon, Department of Chemical and Environmental Engineering, University of Zaragoza, 50009 Zaragoza, Spain

ARTICLE INFO

Article history:
Available online 24 April 2010

Keywords:
CNT growth kinetics
Ni–Mg–Al catalyst
CCVD
Methane
Deactivation

ABSTRACT

In this work, we present the application of a phenomenological kinetic model to the analysis of experimental results obtained with a LDH-based Ni–Mg–Al catalyst during the CCVD of methane. This model takes into account all the main stages implicated in CNT growth: methane decomposition, metal surface carburization, carbon diffusion, CNT nucleation and growth. The main causes of growth cessation, catalyst deactivation and steric hindrance have also been considered.

The effect of the main operational variables, reduction (activation) and reaction temperatures and feed composition (hydrogen and methane composition), have been studied. The model fits very well the data obtained with the studied catalyst at the different operating conditions. As a consequence of the application of the model to the kinetic results, we can describe the influence of the operating conditions on each of the individual stages involved in the CNT formation.

1. Introduction

The catalytic decomposition of hydrocarbons over transition metals, mainly Ni, Fe and Co has been receiving increasing attention as an alternative route to the production of hydrogen and also carbon nanotubes [1–6].

The great potential of new uses of hydrogen is based on the fact that it is a clean fuel that does not emit CO_2 when used in H_2–O_2 fuel cells, it can be stored as a liquid or gas, and it can be distributed via pipelines. Hydrogen has been described as a long-term replacement for natural gas [7]. Therefore, a growing demand is forecast in most industrial and energy sectors, including petroleum refining where the increasing need to process heavy and high-sulphur content crude-oil is accompanied by the lowering of hydrogen co-product in the catalytic reforming process. Steam reforming of methane and other hydrocarbon feedstocks has been the most commonly employed and usually the most economical technology for the production of hydrogen [7,8]. However, this route makes hydrogen an indirect source of CO_2. In addition, the co-product of steam reforming, CO, must be removed by two subsequent steps: water–gas shift and methanation. The complete removal of CO is not economical and therefore the hydrogen thus produced is not suitable for low-temperature fuel cells given that the catalyst is poisoned by CO [1,9]. One of the advantages of catalytic decomposition of methane, also called catalytic chemical vapour deposition (CCVD), is that it avoids direct formation of CO or CO_2 and therefore subsequent steps for CO removal are not needed [1–4]. In addition to hydrogen production, CCVD produces carbon nanotubes, CNTs, and carbon nanofibres, CNFs. Carbon nanofibres have been known for a long time as a problem that often appears during catalytic conversion of carbon containing gases. The recent outburst of interest in this type of nanocarbonaceous material, especially CNTs, derives from their potential for unique applications [10].

One of the most challenging aspects is the complete description of the complex mechanism that controls the growth of CNTs. Thus, there is no general agreement about what the critical steps are. Most authors propose that this mechanism includes hydrocarbon (or another carbon source such as CO) decomposition over the surface on the metallic particles, then carbon diffusion through the particles [10–15] and/or atomic carbon surface transport [16,17] and finally carbon precipitation forming CNTs. Recently [18], we have proposed a model that in addition to the effect of the initial induction period also includes the effect of a reversible deactivation by encapsulating coke. During the initial, and critical, induction period, both the surface carburization of the metallic nanoparticles and the nucleation of CNTs take place, which determines the later growth of CNTs. The main causes of the growth termination are the catalyst deactivation and the steric hindrance to CNT growth [19]. Both phenomena have also been considered in the model as an important part of the description of the growth mechanism [18].

As regards the catalysts used for the CCVD process, we have been investigating for some years the application of hydrotalcite-like compounds as catalytic precursors [4,6,20–23]. Recently [24], we have found that the modification of the Ni–Al catalyst composition,

* Corresponding author. Tel.: +34 976 761157; fax: +34 976 762142.
E-mail address: amonzon@unizar.es (A. Monzón).

0920-5861/$ – see front matter © 2010 Elsevier B.V. All rights reserved.
doi:10.1016/j.cattod.2010.03.065

by inclusion of MgO to obtain Ni–Mg–Al catalysts, notably increases their productivity and stability during the catalytic decomposition of methane. The better performance of Ni–Mg–Al catalysts was explained considering the higher interaction generated between Ni particles and the Mg–Al support, which prevents the formation of large metallic particles, decreasing the encapsulating coke formation and increasing the selectivity to production of carbon nanotubes of multiple-walls (MWNT) [24]. In this work, we present the application of the phenomenological kinetic model [18] to the analysis of experimental results obtained with a LDH-based Ni–Mg–Al catalyst during the CCVD of methane. In particular, we have investigated the effect of the reduction (activation) and reaction temperatures, and of the feed composition (methane and hydrogen concentration). The application of the model allows us to improve our knowledge of the influence of the operating conditions on each of the individual stages involved in the CNT formation.

2. Kinetic model of CNT growth

After the stage of methane decomposition, atoms of carbon and gaseous hydrogen are released over the surface of the Ni nanoparticles. Simultaneously, reversible formation of encapsulating coke occurs partially deactivating the catalyst. In the following sections the kinetic descriptions of these stages are presented.

2.1. Formation of surface carbide and carbon nanotube nucleation

After methane decomposition the remaining carbon atoms react with the metallic nanoparticles at the surface forming a metastable carbide, that in the reaction conditions decomposes leaving carbon atoms at the metallic subsurface [25]. After this decomposition-segregation step, the carbon atoms are introduced inside the metal particles [25], determining the value of the carbon concentration at the carbide-metallic nanoparticle interphase. Other authors [26] consider that the carbon atoms are dissolved on the metallic nanoparticles forming a highly disordered 'molten' layer on their surface, on which carbon diffusivity is much higher. Helveg et al. [16] propose that the growth of CNFs on a Ni–Mg–Al catalyst involves surface diffusion of both carbon and nickel atoms. In any case, we consider that the carbon atoms enter into the metallic nanoparticles through the clean surface (*interface* 1), and that they leave the metallic phase through *interface* 2 when forming the CNT [19]. The driving force for the surface or bulk diffusion from *interface* 1 to *interface* 2 is the difference in chemical potential between the two interfaces. Assuming that the process of nucleation follows an autocatalytic kinetics [19,27], the rate of carburization-nucleation is expressed as [18]:

$$r_S = \frac{dC_S}{dt} = \psi_S \cdot (1 + K_S \cdot C_S) \cdot (C_{S_m} - C_S) \quad (1)$$

where C_S is the concentration of surface carbide and has units of (g C/g cat). The term ψ_S represents the intrinsic *kinetic function of carburization*, and for a given catalyst its value depends on the reaction conditions. C_{S_m} represents the maximum surface carbide concentration attainable on the surface of metallic particles at the side gas phase. The parameter K_S represents the contribution of the autocatalytic effect on the carburization kinetics.

Considering that the reactor operates at low methane conversions, i.e. under differential conditions, the terms ψ_S and K_S can be considered constants, and the analytical solution of Eq. (1) gives:

$$C_S = \frac{C_{S_m} \cdot (1 - \exp(-\psi_C \cdot t))}{(1 + K_S \cdot \exp(-\psi_C \cdot t))}; \quad \psi_C = \psi_S \cdot (1 + K_S \cdot C_{S_m}) \quad (2)$$

2.2. Rate of carbon nanotube growth

When the carbon concentration has reached a certain threshold, nucleation occurs forming graphene caps [28–30]. This fact generates the *interface* CNT-metal, *interface* 2, and the carbon flux is maintained because the nanotube structure provides a thermodynamic sink for the carbon, and as a result the carbon concentration at the *interface* 2 is kept low. The rate of the diffusion-precipitation process determines the rate of formation of carbon nanotubes. In the case of methane decomposition the stoichiometry is $CH_{4(g)} \leftrightarrow C_{(s)} + 2H_{2(g)}$, and therefore the rates of methane conversion, CNT formation, and hydrogen production are directly related by:

$$(-r_{CH_4})_t = (r_{H_2})_t/2 = (r_C)_t = (r_C)_0 \cdot a(t); \quad a(t) = (r_C)_t/(r_C)_0 \quad (3)$$

In this expression, the terms a and $(r_C)_0$ are respectively the catalyst activity and the initial CNT growth rate, i.e. the rate for the fresh catalysts without deactivation. This rate can be expressed in terms of a classical diffusion equation as [31]:

$$\frac{\partial C_C}{\partial t} = D_{C,e} \cdot \nabla C_C \quad (4)$$

Assuming unidirectional diffusion, the initial rate of CNT formation can be calculated as a simplified form of the above equation:

$$(r_C)_0 = \left.\frac{dm_C}{dt}\right|_{t=0} = k_C \cdot (C_S - C_F) \quad (5)$$

The term k_C is the effective coefficient of carbon transport, has units of time^{-1}, and depends on the average size of the metallic crystallites, the metallic exposed area, and the carbon atom diffusivity on the metallic nanoparticles [13,14,19,32,33]. In addition, assuming that the value of C_F is very low compared to the value of C_S, the rate of CNT formation can be expressed as:

$$(r_C)_t = (r_C)_0 \cdot a(t) \cong k_C \cdot C_S \cdot a(t) \quad (6)$$

2.3. Catalyst deactivation

The main causes of catalyst deactivation are fouling by encapsulating coke, sintering (or thermal aging), and poisoning [34]. Therefore, the deactivation rate, $r_d = -da/dt$, must be described according to an appropriate deactivation kinetic model related to the deactivation cause [34–36]. Thus, if the formation of encapsulating coke is partially reversible, the catalyst does not suffer a complete deactivation, maintaining a residual level of activity at steady state. In these conditions, the net rate of activity variation can be expressed as [18,36]:

$$r_d = -\frac{da}{dt} = \psi_d \cdot a^d - \psi_r \cdot (a^{d_m} - a) \quad (7)$$

The terms ψ_d and ψ_r are respectively the "*deactivation and regeneration kinetic functions*", and both also depend on the operating conditions. In addition, the values of the kinetic orders d and d_m are calculated considering the number of sites involved in the controlling step of the main reaction (m), and of the deactivation reaction (h) as follows [18,36]: $d = (m + h - 1)/m$ and $d_m = (m - 1)/m$. For the case of methane decomposition, the assumed values for m and h are 2 and 1, respectively, therefore the kinetic orders will be $d = 1$ and $d_m = 1/2$. In this case, the integration of Eq. (6) gives:

$$a(t) = \left(\frac{\psi_r}{\psi_G} + \frac{\psi_d}{\psi_G} \cdot \exp\left(-\frac{\psi_G}{2} \cdot t\right)\right)^2; \quad \psi_G = \psi_d + \psi_r \quad (8)$$

Finally, substituting Eqs. (2) and (8) into Eq. (6), the amount of CNTs formed over the catalyst can be calculated integrating numer-

ically the following expression:

$$(r_C)_t = \frac{dm_C}{dt} = \left(\frac{j_{C_0}(1-\exp(-\psi_C \cdot t))}{(1+K_S \cdot \exp(-\psi_C \cdot t))}\right) \cdot \left(\frac{\psi_r}{\psi_G} + \frac{\psi_d}{\psi_G} \cdot \exp\left(-\frac{\psi_G}{2} \cdot t\right)\right)^2 \quad (9)$$

where the term j_{C0} is defined as:

$$j_{C_0} = C_{S_m} \cdot k_C \quad (10)$$

j_{C0} has units of (g C/g cat min) and can be considered as the maximum flux of carbon atoms through the catalytic metallic particles.

3. Results and discussion

The main results of the catalyst characterization and of the influence of the reaction conditions have been previously presented [24]. In summary, it was obtained that after calcination at 800 °C, the solid sample contains NiO and non-stoichiometric $NiAl_2O_4$ and $MgAl_2O_4$ spinel phases. After reduction and reaction stages, it is possible to distinguish the peaks corresponding to the metallic Ni^0 and to the graphitic carbon formed on the catalyst during the reaction. Besides, the spinel structure is also detected, which indicates that the catalyst does not suffer a substantial degradation during the reaction. The average size of the Ni^0 crystallites, calculated by means of the Debye–Scherrer equation, is 14.6 nm. An increase in the average size of the metallic Ni crystallites is observed when the reduction temperature rises, indicating metallic phase sinterization after the reduction step. The average sizes calculated for Ni crystallites of Ni–Mg–Al samples are lower than those of Ni–Al catalysts, indicating a higher stabilization of Ni particles on the $MgAl_2O_4$ phase formed in the Ni–Mg–Al sample [24]. This result was also confirmed by TPR results, where a higher reduction temperature of Ni^{+2} species was clearly observed for the Ni–Mg–Al catalyst [24]. Besides, the addition of MgO increases the specific surface BET area (from 92 to 143 m^2/g), which ensures a good dispersion of the active metal and consequently adequate catalyst activity.

Fig. 1 shows two TEM pictures at different magnification of a sample after reaction carried out under the following operating conditions: temperature of reduction: 750 °C, temperature of reaction: 600 °C, feed composition: 5% CH_4, 2% H_2, 93% N_2. These TEM micrographs show that two different types of carbon can be distinguished: multi-wall carbon nanotubes (MWNT) as the main carbonaceous material, and a small fraction of amorphous carbon, which encapsulates the metallic particles hindering the decomposition of the methane, and the subsequent carbon diffusion to form the carbon nanotubes. For a given catalyst, the relative quantities of each type depend on the different operating conditions. The lower the quantity of amorphous carbon formed, the less catalyst deactivation is observed [4]. In addition, metal particles are visible at the tips of some nanotubes suggesting a tip growth mode [10,11,37].

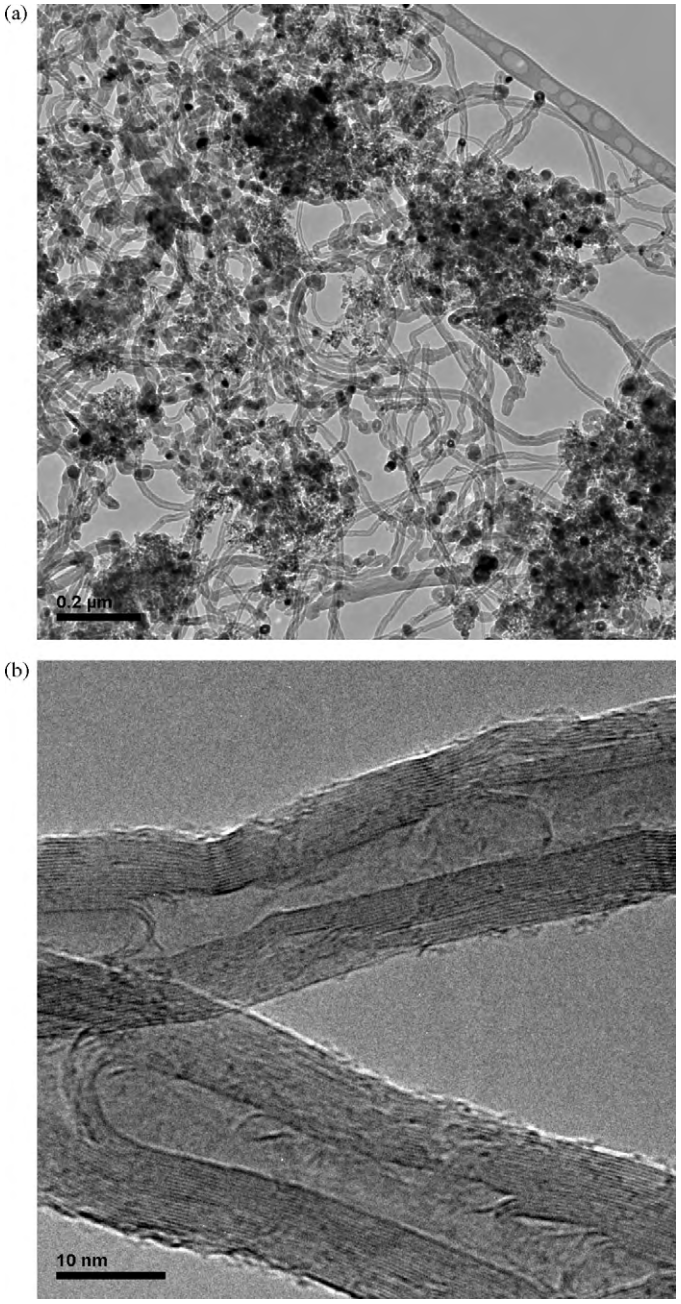

Fig. 1. TEM micrographs of a Ni–Mg–Al sample after CCVD reaction with methane. Operating conditions: temperature of reduction: 750 °C, temperature of reaction: 600 °C, feed composition: 5% CH_4, 2% H_2, 93% N_2.

3.1. Kinetic results and model application

3.1.1. Influence of the reduction temperature

Fig. 2 shows the effect of the reduction temperature, in the range of 650–850 °C, over the evolution of CNT concentration. The operating temperature was 600 °C and the feed composition 5%CH_4/95%N_2. As can be seen in this figure, the amount of CNTs formed over the catalyst at a given reaction time increases with the reduction temperature until a maximum is attained at 750 °C. At higher temperatures the catalyst productivity decreases. The appearance of this maximum is explained considering the effect of two opposite factors. On the one hand, the increase of the reduction temperatures generates a higher number of active sites, i.e. a large number of metallic Ni particles are formed. On the other hand, the use of elevated reduction temperatures gives rise to more intense sinterization of the metallic particles, decreasing the exposed metallic area, and therefore the activity. These assumptions are in accordance with the measurements of the average particle size measured by XRD [24]. According to the results of De Chen et al. [6], there is an optimum Ni particle size that maximizes the carbon yield during the methane decomposition reaction. Thus, Ni particles which are too small show a low growth rate and fast deactivation, and very large Ni crystals have low activity because of the low metallic area. The reduced coking rate on small-sized Ni particles is a consequence of a low driving force for carbon diffusion through the Ni crystals [6]. As a consequence, the surface coverage

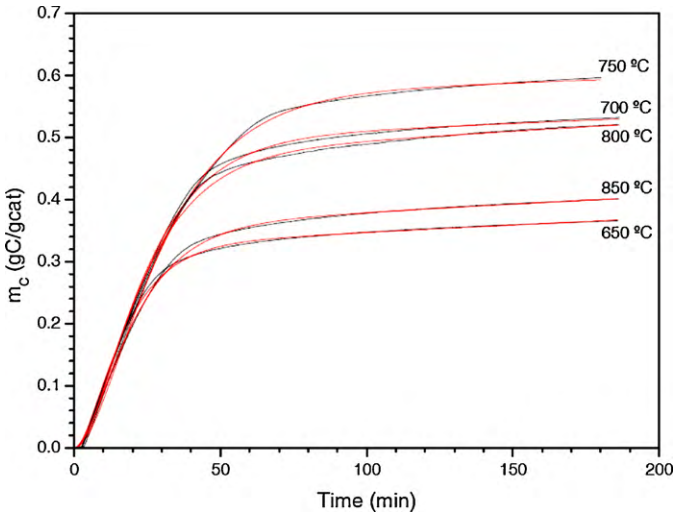

Fig. 2. Influence of reduction temperature over the rate of CNTs formation. Red line: model prediction, black line: experimental data. (For interpretation of the references to color in this figure legend, the reader is referred to the web version of the article.)

of carbon increases, which enhances the formation of encapsulating coke and thus deactivation.

With respect to the model application, in Fig. 2 it can be seen that for all the reduction temperatures studied, the model fits very well the development of CNT concentration along the reaction time. The calculations of the kinetic parameters have been made by a non-linear regression fitting routine implemented in Excel. The objective function minimized is the sum of the squared residuals of the m_C. The numerical integration of Eq. (9) has been made by a standard Runge-Kutta of 4th order routine.

The values of the calculated parameters are represented in Fig. 3a and b. The observed evolution of the parameters with the reduction temperature is consistent with the presence of a maximum CNT production when the catalyst was reduced at 750 °C. Thus, the values of the more influential parameters for the CNT growth, j_{C0} and ψ_d, show a maximum and a minimum respectively, Fig. 3a and b. Therefore, according to the proposed model, the increase in the reduction temperature up to 750 °C enhances the carbon diffusivity and, at the same time, partially inhibits the deactivation of the metallic particles. At temperatures above 750 °C, the deactivation is enhanced and simultaneously the flux of carbon atoms is decreased. As discussed earlier, these facts are governed by the crystallite size distribution obtained after each reduction treatment. The results shown in Fig. 3b also indicate that the variation of ψ_r is coupled to the variation of ψ_d. This is probably due to the difficulty of evaluating ψ_r when the duration of the experiments is not very long. In fact, according to the proposed model, the value of ψ_r determines the residual activity of the catalyst at infinite time.

With respect to the carburization parameters, K_S and ψ_S, all the experiments have been fitted assuming the same value of K_S. Therefore, the whole influence of reduction temperature over the carburization rate is accumulated over ψ_S, showing a minimum value at 750 °C. However, given that the value of ψ_S is four orders of magnitude lower than that of j_{C0}, Fig. 3a, any variation of ψ_S is more than compensated for by the changes in j_{C0}. This explains, for example, that in spite of the fact that the carburization rate decreases in the interval from 650 to 750 °C, the rate of CNT formation increases in the same interval.

3.1.2. Influence of the reaction temperature

The results relating to the effect of the reaction temperature over the carbon productivity of the catalyst are presented in Fig. 4. In the complete range of temperatures studied, a rapid increase in

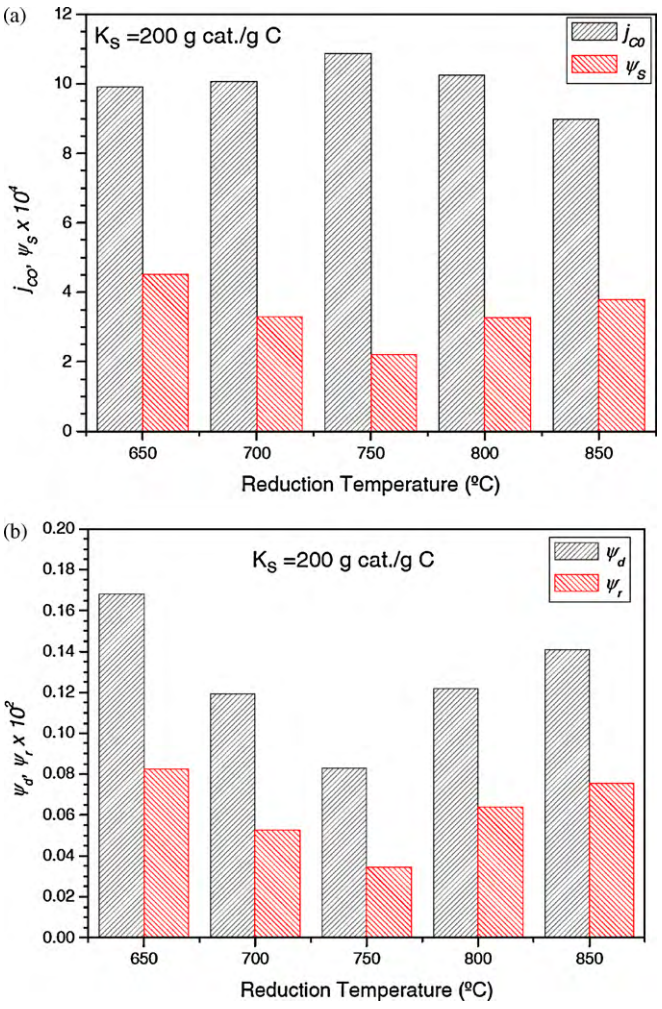

Fig. 3. Influence of reduction temperature on the kinetic model parameters. (a) j_{C0} and ψ_S. (b) ψ_d and ψ_r.

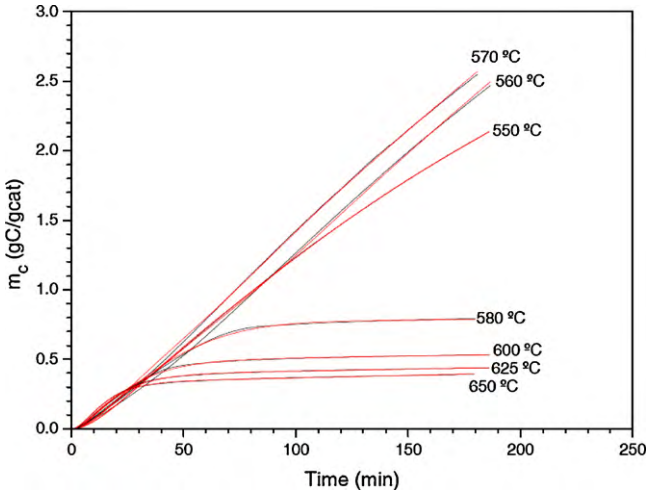

Fig. 4. Influence of reaction temperature over the rate of CNTs formation. Red line: model prediction, black line: experimental data. (For interpretation of the references to color in this figure legend, the reader is referred to the web version of the article.)

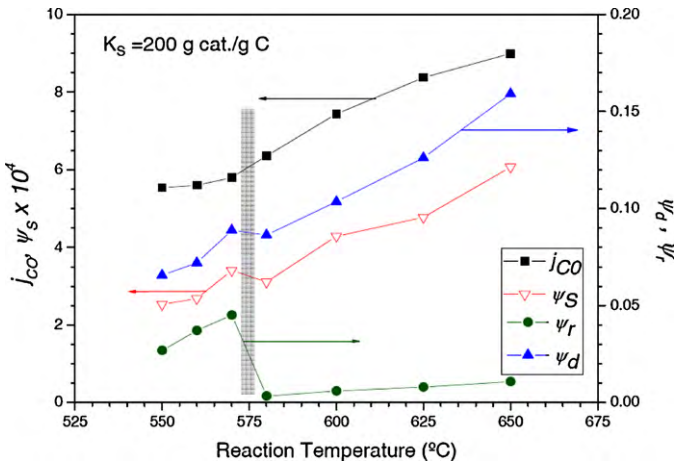

Fig. 5. Influence of reaction temperature on the kinetic model parameters.

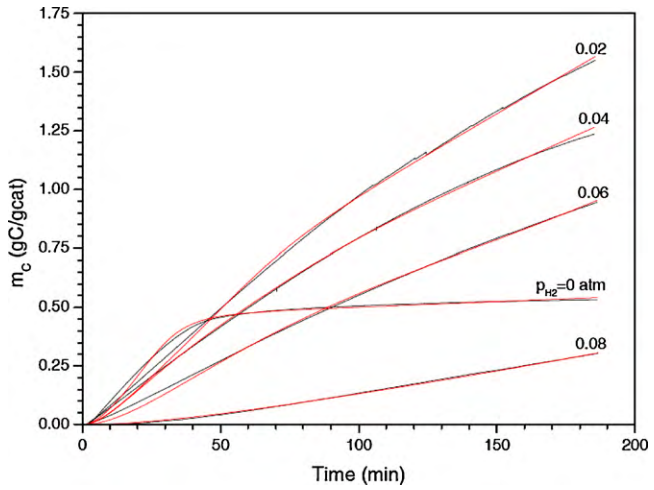

Fig. 6. Influence of hydrogen concentration over the rate of CNTs formation. Red line: model prediction, black line: experimental data. (For interpretation of the references to color in this figure legend, the reader is referred to the web version of the article.)

the reaction rate is observed, calculated as the slope of the m_C vs. *time* curves, until a maximum value is reached. After the appearance of this maximum, the deactivation of the catalyst becomes relevant at temperatures above 570 °C. Then a continuous decrease in the carbon formation rate is observed. However, at low temperatures (below 570 °C) the deactivation is almost negligible, and the CNT content vs. time curves are almost straight lines (Fig. 4). The appearance of this critical temperature is a consequence of the competition between the carbon diffusion through the particles that finally form the carbon nanofibres, and the formation of encapsulating coke responsible for the deactivation [10].

As in the previous case, the application of Eq. (9) to the experimental data given in Fig. 4 allows very good fits to be obtained for all the temperatures studied. The values of the calculated parameters are represented in Fig. 5. The model is able to fit the cases both where there is no catalyst deactivation and the opposite where the catalyst suffers a strong loss of activity at temperatures above 570 °C. The evolution of the values attained for the parameters confirms the important change that the catalyst behaviour undergoes at 570 °C. As expected, in all cases the values of the parameters increase with the temperature, but at 570 °C the above-mentioned transition between the two zones appears. As can be seen in Table 1, this transition is characterized by a change in the Arrhenius parameters.

From the data shown in Table 1 and in Fig. 5, it can be seen that in spite of the strong diminution of catalyst productivity, the parameter j_{C0} continuously increases over the whole interval of temperatures studied. For this parameter the activation energy increases from 13.5 to 32.1 kJ/mol, indicating that at the HT temperature zone the growth of CNT is less favoured. The low values of activation energy estimated for j_{C0} seem to indicate that the mechanism of carbon migration is surface diffusion [16,31].

The activation energy of ψ_d decreases from 87.4 to 56.7 kJ/mol, indicating that at the HT zone the catalyst is more prone to deactivation. The values of activation energies for ψ_r are higher than those corresponding to ψ_d. For this reason, the gasification of encapsulating coke on the surface of metallic nanoparticles is a more difficult process than their formation under the operating conditions studied. In addition, at the HT zone the pre-exponential factor of ψ_r decreases by almost 3 orders of magnitude with respect to the LT zone, see Table 1. This fact shows that, in addition to the increase in the intrinsic rate of catalyst deactivation, the strong decrease in the rate of regeneration is also responsible for a large part of the loss of catalyst productivity observed at the HT zone.

With respect to the intrinsic rate of carburization, ψ_S, the activation energy decreases from 85.7 to 58.6 kJ/mol, and simultaneously the pre-exponential factor increases by almost 200 times. Both facts indicate that at the HT temperature zone, the surface carburization of metallic nanoparticles is favoured. The observed decrease of the K_S parameter has little significance. In this case, all the experiments have also been fitted assuming a constant value of K_S.

Table 1
Activation energies and pre-exponential factors of the kinetic parameters at low (L.T.) and high (H.T.) temperatures.

Parameter	$\ln(k_0)$ (L.T.)	E_a (L.T.) (kJ/mol)	$\ln(k_0)$ (H.T.)	E_a (H.T.) (kJ/mol)
j_{C0}	3.7 ± 0.2	13.5 ± 0.6	6.4 ± 0.6	32.1 ± 2.3
ψ_S	4.2 ± 0.3	85.7 ± 2.8	9.4 ± 0.8	58.6 ± 3.1
ψ_d	10.0 ± 0.7	87.4 ± 5.0	5.5 ± 0.4	56.7 ± 2.8
ψ_r	16.1 ± 1.3	150.8 ± 6.1	9.3 ± 0.7	106.1 ± 4.1

3.1.3. *Influence of feed composition*

The effect of the hydrogen and methane partial pressures on the evolution of CNT concentration is presented in Figs. 6 and 7, respectively. As can be seen in Fig. 6, the presence of hydrogen in the feed significantly changes the catalyst performance, decreasing or even avoiding catalyst deactivation. Thus, when no hydrogen is

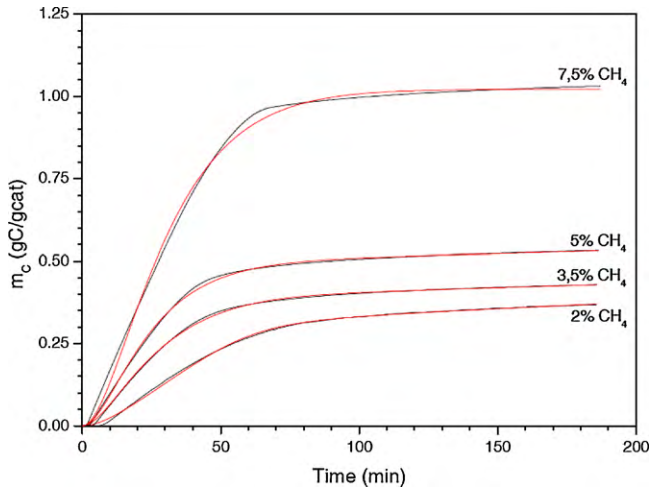

Fig. 7. Influence of methane concentration over the rate of CNTs formation. Red line: model prediction, black line: experimental data. (For interpretation of the references to color in this figure legend, the reader is referred to the web version of the article.)

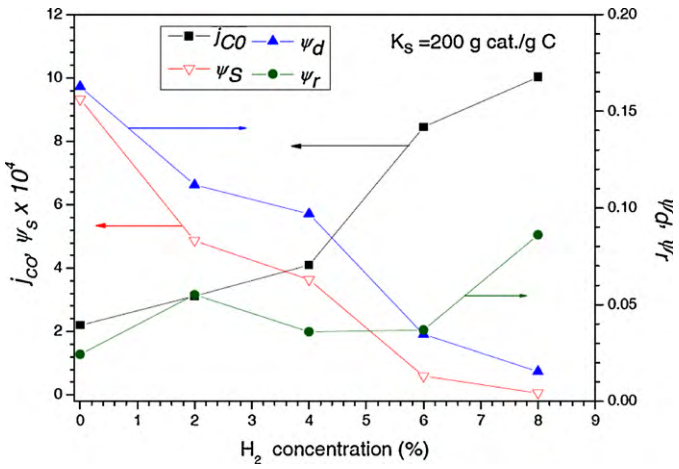

Fig. 8. Influence of hydrogen concentration on the kinetic model parameters.

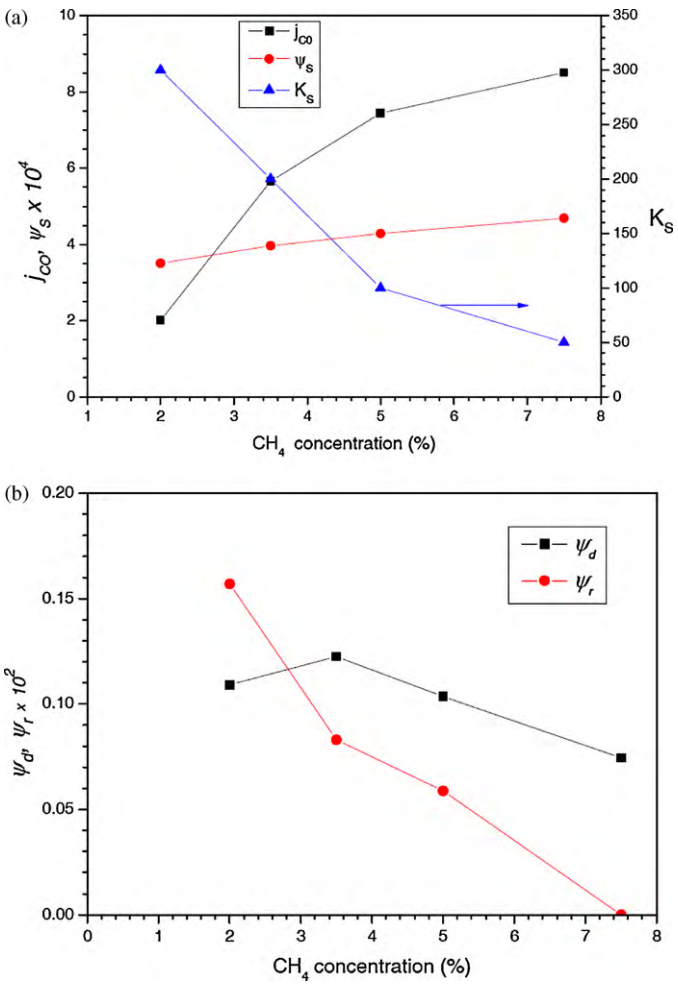

Fig. 9. Influence of methane concentration on the kinetic model parameters. (a) j_{C0}, ψ_S and K_S (b) ψ_d and ψ_r.

fed to the reactor, the reaction rate increases very quickly but the loss of activity is also very significant. As the hydrogen concentration increases, the initial augmentation of the reaction rate is less pronounced, but the deactivation is also lower because hydrogen averts the formation of encapsulating coke. However, if the hydrogen concentration is too high, due to the competition between H_2 and CH_4 for the metallic surface sites a diminution in the net reaction rate is observed [4,13,14].

As regards the effect of p_{CH_4}, the results show that an increase in methane concentration boosts the reaction rate, but the residual rate after the deactivation period is similar in all the experiments (Fig. 7). Therefore, as the rate of CNT growth increases, the deactivation will also be more marked, attaining the same remaining catalyst activity. These facts can be explained considering that at higher methane concentrations there is an improvement in the carbon diffusion and CNT precipitation. However, the increase of p_{CH_4} also promotes the formation of carbon species which encapsulate and deactivate the surface of the metallic nanoparticles [10,14,38–40].

The application of the kinetic model for these sets of experiments is also very satisfactory, obtaining an excellent concordance between the experimental data and the model calculations. The values of the kinetic parameters are represented in Figs. 8 and 9a and b. Thus, Fig. 8 shows that as the p_{H_2} increases the values of j_{C0} and ψ_r also increase, but the parameters ψ_S and ψ_d diminish. These results are in full agreement with the above described role played by hydrogen in this reaction, showing the validity of the kinetic model used. Regarding the effect of p_{CH_4} on the kinetic parameters, Fig. 9a and b indicate that the higher the p_{CH_4}, the higher the value of j_{C0} and ψ_S. However, the parameter K_S decreases. The variation of ψ_d and ψ_r can be explained considering that at high methane concentrations, the inhibition of the regeneration step is more important than the increase in the deactivation.

The combined evolution of K_S (decrease) and ψ_S (slight increase) explains the decrease in the initial induction period observed in Fig. 7 as the p_{CH_4} increases. The early stages of carburization-CNT nucleation occur during the induction period, characterized by a very low CNT formation rate. According to the proposed model, their extent depends on the parameters K_S and ψ_S [18]. Thus, the lower the number of CH_4 molecules in the gas phase, the more difficult is the carburization-nucleation step, and therefore more time is needed to complete this stage. Therefore, the carbon atoms left at the Ni metallic surface will produce encapsulating coke given that their low surface concentration is not sufficiently high to carburize the Ni particles. This fact could explain the deactivation observed even at low methane concentrations. According to the results presented in this work, the operational variable that mainly affects the induction period is the methane concentration. The other variables studied do not seem to affect the duration of the induction period.

4. Conclusions

We have shown that the phenomenological model used provides a good fit with all the experimental data obtained with a LDH-based Ni–Mg–Al catalyst during the CCVD of methane.

The values of the parameters obtained are consistent with the evolution of the CNT production curves in all the cases studied. Thus, with respect to the influence of the reduction temperature, it was obtained that the CNT production goes through a maximum at 750 °C as a consequence of the different Ni particle size and degree of reduction obtained. The model accurately explains this result considering that the values of the diffusion rate (j_{C0}) and the deactivation rate (ψ_d) show a maximum and a minimum, respectively.

The appearance of a critical operation temperature (570 °C for this catalyst) below which there is no deactivation is a result of the competition between the carbon diffusion through the nanoparticles, and the formation of encapsulating coke. The model is able to fit the results at two zones, at low and high temperature, stressing the change that the catalyst behaviour undergoes at the critical temperature. This transition is characterized by a change in the activation energies of the kinetic parameters.

Finally, the effect of the feed composition on the kinetic parameters shows that as the p_{H_2} increases, the CNT productivity passes

through a maximum due to the competition between H_2 and CH_4 for the metallic surface sites. In this case the model predicts a continuous increase of j_{C0} and ψ_r while ψ_S and ψ_d diminish. The coupling effect of the kinetics parameters is perfectly able to explain the maximum.

Regarding the methane effect, it is observed that an increase in methane concentration raises both the CNT growth rate and the deactivation rate. In addition, a shortening of the induction period was observed. All these effects are also well explained by the model. As a relevant result, it is worth noting that the combined decrease of K_S and increase of ψ_S explains the observed decrease in the initial induction period. According to the results presented in this work, the operational variable that mainly affects the induction period is the methane concentration. The rest of the studied variables do not seem to affect the duration of the induction period.

Acknowledgements

The authors acknowledge financial support from MICINN (Spain)-FEDER, Project CTQ 2007-62545/PPQ, and the Regional Government of Aragón, Departamento de Ciencia, Tecnología y Universidad, Project CTP P02/08.

References

[1] N.Z. Muradov, T.N. Veziroglu, Int. J. Hydrogen Energy 30 (2005) 225.
[2] N.Z. Muradov, Int. J. Hydrogen Energy 26 (2001) 1165.
[3] T. Zhang, M.D. Amiridis, Appl. Catal. A 167 (1998) 1161.
[4] J.I. Villacampa, C. Royo, E. Romeo, J.A. Montoya, P. del Angel, A. Monzón, Appl. Catal. A 252 (2003) 363–383.
[5] M. Pérez-Cabero, E. Romeo, C. Royo, A. Monzón, A. Guerrero-Ruiz, I. Rodríguez-Ramos, J. Catal. 224 (2004) 197.
[6] K.O. De Chen, E. Christensen, Z. Ochoa-Fernández, B. Yu, N. Tøtdal, A. Latorre, A. Monzón, Holmen, J. Catal. 229 (2005) 82.
[7] J.N. Armor, Appl. Catal. A 176 (1999) 159.
[8] J.M. Abrardo, V. Khurana, Hydrocarbon Proc. 79 (1995) 43.
[9] M. Steinberg, H.C. Cheng, Int. J. Hydrogen Energy 14 (1989) 797.
[10] K.P. de Jong, J.W. Geus, Catal. Rev. Sci. Eng. 42 (2000) 481.
[11] D.L. Trimm, Catal. Rev. Sci. Eng. 16 (1977) 155.
[12] I. Alstrup, M.T. Tavares, J. Catal. 139 (1993) 513.
[13] J.-W. Snoeck, G.F. Froment, M. Fowles, J. Catal. 169 (1997) 240.
[14] J.-W. Snoeck, G.F. Froment, M. Fowles, J. Catal. 169 (1997) 250.
[15] J.A. Rodríguez-Manzo, M. Terrones, H. Terrones, H.W. Kroto, L. Sun, F. Banhart, Nat. Nanotechnol. 2 (2007) 307.
[16] S. Helveg, C. Lopez-Cortes, J. Sehested, P.L. Hansen, B.S. Clausen, J.R. Rostrup-Nielsen, F. Abild-Pedersen, J.K. Nørskov, Nature 427 (2004) 426.
[17] M. Lin, J.P.Y. Tan, Ch. Boothroyd, K.P. Loh, E.S. Tok, Y.-L. Foo, Nano Lett. 6 (2006) 449.
[18] N. Latorre, E. Romeo, T. Ubieto, C. Royo, J.I. Villacampa, A. Monzón, J. Phys. Chem. C 114 (2010) 4773.
[19] A. Monzon, G. Lolli, S. Cosma, M. Sayed-Ali, D.E. Resasco, J. Nanosci. Nanotechnol. 8 (2008) 6141.
[20] A. Monzón, N. Latorre, T. Ubieto, C. Royo, E. Romeo, J.I. Villacampa, L. Dussault, J.C. Dupin, C. Guimon, M. Montioux, Catal. Today 116 (2006) 264.
[21] L. Dussault, J.C. Dupin, N. Latorre, T. Ubieto, L. Noé, M. Monthioux, E. Romeo, C. Royo, A. Monzón, C. Guimon, J. Phys. Chem. Solids 67 (2006) 1162.
[22] L. Dussault, J.C. Dupin, C. Guimon, M. Monthioux, N. Latorre, T. Ubieto, E. Romeo, C. Royo, A. Monzón, J. Catal. 251 (2007) 223.
[23] P. Benito, M. Herrero, F.M. Labajos, V. Rives, C. Royo, N. Latorre, A. Monzón, Chem. Eng. J. 149 (2009) 455.
[24] N. Latorre, J.I. Villacampa, T. Ubieto, E. Romeo, C. Royo, A. Borgna, A. Monzón, Top. Catal. 51 (2008) 158.
[25] I. Alstrup, J. Catal. 109 (1988) 241.
[26] A.A. Puretzky, D.B. Geohegan, S. Jesse, I.N. Ivanov, G. Eres, Appl. Phys. A 81 (2005) 223.
[27] Ch. Soman, T. Giorgio, Nano Res. 2 (2009) 78.
[28] T. Yamada, A. Maigne, M. Yudasaka, K. Mizuno, D.N. Futaba, M. Yumura, S. Iijima, K. Hata, Nano Lett. 8 (2008) 4288.
[29] J. Zhao, A. Martinez-Limia, P.B. Balbuena, Nanotechnology 16 (2005) S575.
[30] F. Ding, A. Rosén, K. Bolton, Comp. Mater. Sci. 35 (243) (2006) 6.
[31] F. Le Normand, V. Švrček, A. Senger, T. Dintzer, C. Pham-Huu, J. Phys. Chem. C 113 (2009) 14879.
[32] J.R. Rostrup-Nielsen, J. Catal. 27 (1972) 343.
[33] J.R. Rostrup-Nielsen, D.L. Trimm, J. Catal. 48 (1977) 155.
[34] C.H. Bartholomew, Appl. Catal. A: Gen. 212 (2001) 17.
[35] A. Monzón, E. Romeo, A. Borgna, Chem. Eng. J. 94 (2003) 19.
[36] J.C. Rodriguez, J.A. Peña, A. Monzón, R. Hughes, K. Li, Chem. Eng. J. 58 (1995) 7.
[37] R.T.K. Baker, Carbon 27 (1989) 31.
[38] Y. Li, J. Chen, L. Chang, Appl. Catal. A 163 (1997) 45.
[39] T.V. Choudhary, C. Sivadinarayana, C.C. Chusuey, A. Klinghoffer, D.W. Goodman, J. Catal. 199 (2001) 9.
[40] M.L. Toebes, J.H. Bitter, A. Jos Van Dillen, K.P. de Jong, Catal. Today 76 (2002) 33.